Design of a Novel Hypersonic Inflatable Aerodynamic Decelerator for Mars Entry, Descent, and Landing

Team members

Lin Li

Grant Rossman

Nathaniel Skolnik

Hiromasa Kamezawa

Alex Longo

Georgia Institute of Technology

Faculty Advisors

Dr. Robert D. Braun and Dr. Brandon Sforzo

Entry, descent, and landing (EDL) is especially challenging on Mars because the atmosphere is too thin to provide substantial deceleration but thick enough to generate significant heating during the reentry phase. As a result, innovative ideas are required to enable future high-mass Mars landing missions. One such promising approach is to use an inflatable aerodynamic decelerator (IAD). Compared with traditional rigid aeroshells, IADs are made of lightweight, flexible materials that can be folded into a smaller volume in the rocket payload fairing and inflated prior to atmospheric entry. Such IADs are able to reduce the ballistic coefficient and peak heating, providing an opportunity to land at higher surface elevations on Mars. Currently, NASA Langley Research Center is investigating the development of Hypersonic Inflatable Aerodynamic Decelerators (HIADs) to enable future large robotic and human exploration missions. Much of the previous work performed on HIADs has focused on symmetric shapes that fly through the atmosphere with ballistic trajectories or trajectories with low lift-to-drag ratios accomplished via CG-offset. The present investigation assesses the technical feasibility of a novel HIAD concept that can vary lift-to-drag ratios between 0.2 and 0.5, is aerodynamically stable between 0.6 km/s and 6.5 km/s, is extensible to aeroshell diameters of 15 to 20 meters, and possesses a smooth outer mold line to avoid localized heating.

I. Introduction

Entry, descent, and landing (EDL) is especially challenging on Mars due the nature of the planet. The atmosphere on Mars is too thin (approximately 1% of Earth's density) to provide substantial deceleration, but thick enough to generate significant heating during the reentry phase. As a result, Mars entry vehicles have been constrained to land at lower surface elevations. Past successful Mars landers have relied on Viking heritage technologies that are capable of delivering landed payloads of 0.9 (metric tons) at MOLA elevations below 0 (km) [1,2]. The most recent example was the Mars Science Laboratory (MSL) mission in 2012. Future human exploration missions will require much larger payload masses ranging from 20 (metric tons) to as much as 80 (metric tons) per landing event [1]. These missions will likely require the deployment of much larger drag devices in order to manage the ballistic coefficient. Such requirements cannot be achieved with Viking EDL technology since the maximum diameter of the rigid aeroshell is constrained by the diameter of the launch vehicle fairing.

As a result, innovative ideas are being studied in order to enable future Mars missions. One such promising approach is to use an inflatable aerodynamic decelerator (IAD), originally developed in the 1960s [3-9]. Compared with traditional rigid aeroshells, IADs are made of lightweight flexible materials that can be packaged into a smaller volume in the rocket fairing and inflated upon reentry. Such IADs are able to reduce the ballistic coefficient and peak heating, providing an opportunity to land at higher surface elevations on Mars. Currently, NASA Langley Research Center is investigating the development of Hypersonic Inflatable Aerodynamic Decelerators (HIADs) to enable future large robotic and human exploration missions. Most past work on HIADs has focused on symmetric shapes that either fly ballistically or at relatively low lift-to-drag ratios with a modest cg-offset. Many ground tests and flight-tests have been conducted to mature HIAD technology [10-16].

Lifting trajectories allow for shallower trajectories, which reduce the peak heat rate and peak deceleration, as well as expand cross-range capabilities and improve landing accuracy. The most common method of generating lift for an axisymmetric entry vehicle is to use a center-of-gravity (CG) offset in order to fly at the desirable angle of attack. This approach was used, for example, by the Mars Science Laboratory mission. However, achieving a L/D ratio in this manner is costly from a mass and packaging perspective. Therefore, it is important to investigate alternative means of generating lift. One such alternative is to utilize an asymmetric entry body.

II. Technical, Scientific Evaluation and Rationale of Proposed Concept

A. Aeroshell Configuration

One of the most difficult objectives in the Big Idea Challenge is to design a HIAD with a modulated lift-to-drag ratio (L/D) between 0.2 and 0.5. Harper has performed analysis on the use of a shifted, asymmetric HIAD for future Mars missions, which allows higher L/D with relatively small angles of attack [17]. This greatly increases vehicle landing mass capabilities and allows the CG location to move in order to satisfy static stability about the pitch axis. In this investigation, a "100% shifted HIAD" design was chosen for analysis because of its ability to produce the highest L/D values within the shifted HIAD family [18]. In order to meet the design objectives and constraints set forth by the Big Idea Challenge, the 100% shifted HIAD design was redesigned and reworked. A series of novel concepts presented in this technical paper allow for this novel HIAD design to meet performance evaluation criteria, design constraints, and construction feasibility goals. Among the many design variables, maximum L/D was given significant focus. The appropriate HIAD shape was determined by conducting a thorough search of the geometry design space. As an addition to the 100% shifted HIAD design, the team inserted a common cylindrical payload fairing (similar to the IRVE-3 centerbody) extending directly backwards from the rigid heatshield just beyond the depth of the largest diameter tori. The benefits of adding this cylindrical payload fairing are many: supports rigid attachments of tori, provides a protected volume to insert the payload, has the ability to support structural loads if needed, and supports the attachment and function of a viable RCS thruster system. A rigid core aeroshell caps one end of the cylindrical payload fairing while tori and fabric are attached where the rigid core aeroshell and the fairing meet.

B. Aerodynamic Analysis Method

The competition requirements specify that the HIAD concept must achieve aerodynamic stability for velocities between 6.5 (km/s) to 0.6 (km/s). In the Martian atmosphere, these correspond to Mach numbers between 27.3 and 2.52, respectively, for atmospheric properties at 30,000 (m) [19]. Therefore, it can be assumed that the HIAD is primarily operating in a hypersonic regime and a Modified-Newtonian aerodynamic simulation can be used to calculate aerodynamic forces within the velocity window of interest [20]. This aerodynamic simulation was a Computational Fluid Dynamics (CFD) simulation created for this investigation to generate aerodynamic properties of the proposed HIAD concept. The following analysis assumes the ratio of specific heats (γ) in the Martian atmosphere to be 1.28 and independent of altitude [21, 22]. Throughout the geometry selection process, the Mach number was assumed to be 20. Because C_{Pmax} can be considered as constant in the hypersonic flow region, this assumption is reasonable.

C. HIAD Configuration

The HIAD geometry was determined by performing a thorough search of the geometry design space. Design constraints for feasible configurations include a required L/D of 0.5, a CG location that is inside the cylindrical payload fairing, and static pitch stability is achieved. The objective was to minimize the associated trim angle-of-attack corresponding to each feasible design. Choosing a configuration with a smaller trim angle-of-attack is desirable because it requires less ballast mass, allows greater payload volume flexibility, and reduces aerothermal and lateral aerodynamic loading on the leeside of the HIAD [18]. The coordinate system shown in Figure 1 was used throughout this paper.

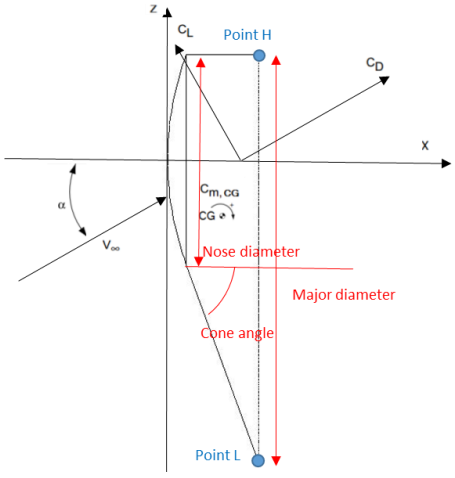

Figure 1: Aerodynamic Forces Exerted on the Vehicle in Body Coordinates

1. Optimization with Taguchi Orthogonal Experimental Design

The cone angle, nose diameter, and base diameter are the three design variables used to define the geometry shown in Figure 1. Through use of a Taguchi L9 orthogonal array [23], this optimization can be performed by assessing the 9 cases shown in Table 1. For each case, Modified Newtonian

aerodynamic analysis was performed at Mach 20 and at 5° angle of attack increments from -30° to 10°. As can been seen in Table 1, Case 6 was the best candidate because it has a minimum angle of attack at which it can achieve an L/D of 0.5. However, this geometry did not meet the pitch static stability requirements, so it was considered infeasible. As such, Case 5 was selected because it generates sufficient L/D with a shallow angle-of-attack of -25°.

Additionally, two trends were observed from the optimization process. First, the cone angle is the most influential variable on L/D. Second, while a larger base diameter and smaller nose diameter could generate larger L/D, a HIAD configuration without static pitch stability may result.

Table 1: Configuration of HIAD Cases and L/D Results

Configs.	Cone Angle (°)	Major Diameter (m)	Nose Diameter (m)	Min. α_{trim} for L/D > 0.5 (°)	L/D at α_{trim}
Case 1	50	15	7	---	---
Case 2	50	17.5	8	---	---
Case 3	50	20	9	---	---
Case 4	65	15	8	-25	0.505
Case 5	65	17.5	9	-25	0.509
Case 6	65	20	7	-20	0.500
Case 7	80	15	9	-30	0.584
Case 8	80	17.5	7	-25	0.500
Case 9	80	20	8	-25	0.500

2. Refined Optimization on Cone Angle

To determine an even more attractive geometry, a second optimization was performed using Case 5 as the baseline. Because the vehicle's cone angle most strongly influences L/D, it was varied between 60° and 75°, in 5° increments, while fixing the major diameter and nose diameter specified by Case 5. A Modified-Newtonian aerodynamic analysis was performed on each shape in Table 2. Case 5-3 was selected as the best candidate because it produced the highest L/D at an angle-of-attack of -25°.

Table 2: Downselection of HIAD Cases and L/D Results

Configs.	Cone Angle (°)	Major Diameter (m)	Nose Diameter (m)	Min. α_{trim} for L/D > 0.5 (°)	L/D at α_{trim}
Case 5-1	60	17.5	9	-30	0.532
Case 5-2	65	17.5	9	-25	0.509
Case 5-3	70	17.5	9	-25	0.511
Case 5-4	75	17.5	9	-25	0.505

After selecting the geometry defined by Case 5-3, additional CFD analysis was performed to find the trim angle-of-attack required to achieve an L/D of exactly 0.5. The Case 5-3 configuration was shown to provide an L/D of exactly 0.5 at a trim angle-of-attack of -24.1°.

3. Pitch Static Stability Analysis

For the selected Case 5-3 configuration, the potential location of the center-of-gravity (CG) was determined and a resulting static stability analysis about the pitching axis was carried out. The CG trim line was determined by examining many points on the interior of the cylindrical payload fairing. For each point, the coefficient of the pitching moment and its slope were determined. Static stability about the pitch axis is defined to satisfy the following two requirements shown in Equation 1 and Equation 2:

$$C_m = 0.00 \quad (1)$$

$$C_{m_\alpha} < 0.00 \quad (2)$$

Figure 2 shows three CG trim lines located 2 (m), 2.5 (m), and 3 (m) below the centerline of the cylindrical payload fairing with a radius of 4.5 (m). The following two trends can be seen in Figure 2:

1. As the CG moves downward in the negative z-direction, the C_m increases.
2. As the CG moves backward in the positive x-direction, the C_m decreases.

It is interesting to note that the rate of change of C_m is faster when the CG is moved in the z-direction when compared with the x-direction. The selected CG trim line was determined to be approximately $z = -2.66$ (m). The corresponding baseline CG location was calculated to be approximately (x,y,z)=(2.34, 0, -2.66). When compared with the 4.5 (m) radius of the cylindrical payload fairing, this CG location was found to be located 59% of the distance between the fairing's centerline and its parallel exterior line. The x component of the CG location was chosen as the point half-way between the payload fairing's nose and tail assuming that the fairing has the same height as the shifted HIAD. The z component of the CG location was determined by the selected CG trim line. The final result of the static stability analysis about the pitch axis is shown in Figure 3. The configuration was determined to be statically stable about the pitch axis at its trim angle-of-attack of -24.1° at Mach 20. Figure 4 shows that pitch static stability was also confirmed at Mach 2.5. Therefore, the Mach number doesn't affect the vehicle's static stability about the pitch axis in this Modified Newtonian aerodynamic analysis.

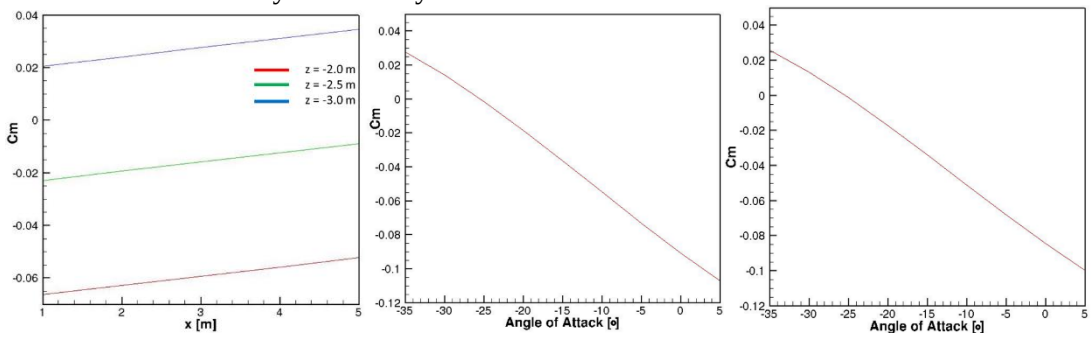

Figure 2: Pitching Moment Coefficient (C_m) with Potential C.G. Locations (Left)
Figure 3: $C_m$vs. Angle-of-Attack with C.G. Located at (x,y,z) = (2.34,0,-2.66) (Center)
Figure 4: $C_m$vs. Angle-of-Attack with C.G. Located at (x,y,z) = (2.34,0,-2.66) for Mach 2.5 (Right)

III. Feasibility of Proposed Concept of Idea, Design Simplicity, Required System Mass, and Extensibility to Large Scale Operation

A. Mass vs. Complexity Study

The asymmetric HIAD design chosen for detailed analysis has a 9 m diameter rigid nose cone (D_N), 70 degree cone angle (θ), and 17.5 (m) overall major diameter (D_0). This analysis focused on determining the total number of tori that would be employed in the final design based on two criteria: design simplicity and decelerator system mass. Minimizing the decelerator system mass is equivalent to minimizing the inflatable structure mass because the mass of the rigid nose cone structure and thermal protection system is fixed for a given decelerator design. Design simplicity was assumed in this analysis to be proportional to the number of components that are used to construct the inflatable structure, and therefore, was equivalent to the total number of tori. The two criteria were combined in an overall objective function by normalizing both quantities with respect to their maximum achieved values and summing them with equal weight, as described in Equation 3. The number of tori used in the final configuration was determined by the design that minimized the overall objective function. The sensitivity to different weightings of mass or simplicity on the objective function was also investigated to understand its effect on the final design parameters.

$$f(\#\ of\ tori) = \frac{mass(i)}{\max(mass)} + \frac{tori\ \#\ (i)}{\max(tori\ \#)} \tag{3}$$

The inflatable structure mass consisted of two major components: the fabric and gas mass. It was assumed that Kevlar would be used to construct the tori and FlexShell cover, the same material that is used on the symmetric stacked tori configuration at NASA Langley Research Center [24]. Kevlar material properties

are available from DuPont technical guides [25]. The tori inflation gas was assumed to be air with the inflation pressure determined based on the 6 (m) HIAD wind tunnel testing [26]. A summary of the parameters used in the inflatable structure mass calculation is shown in Table 3. Additionally, the maximum torus diameter was limited to 1 (m) and the minimum torus diameter was limited to 0.2 (m) to account for reasonable manufacturing capabilities. Designs were also limited to a maximum of 15 tori to bound the complexity.

Table 3: Variable Values for Inflatable Structural Mass Calculation

Gas Density (D_gas) $\left(\frac{kg}{m^3}\right)$	Inflation Pressure (psi)	Fabric Density (D_fab) $\left(\frac{kg}{m^3}\right)$	Fabric Thickness (t) (mm)
1.2922 @ 1 atm	15	1150	1

The mass calculations were performed in Matlab, initially determining the tori minor diameter. Because the tori lay tangent to each other along the shortest edge (L) of the decelerator, the minor diameter (minor diameter of torus) ($2 * r$) could be calculated by dividing the length L by the number of tori, as seen in Figure 5. L could be calculated based on θ, D_N, and D_0, described in Equation 4a. Once r was calculated, their major diameters (major diameter of torus) ($2 * R$) could be determined which then allowed for the calculation of the tori surface area and volume, seen in Equation 4b-4e and Figure 6. In addition, the minimum required payload packing density could also be calculated to verify the feasibility of the design. The calculations assumed that the payload has a cylindrical shape, is located behind the rigid nose cone, and that the length of the payload is the same as L. The payload width was determined by the difference between D_N and twice r, as shown in Equation 5.

$$Shortest\ Edge\ (L) = \frac{(D_0 - D_N)}{\tan(\theta)} \tag{4a}$$

$$R(i) = \frac{1}{2} * (D_N + center\ x\ locaton\ of\ torus\ (i) * \tan(\theta) + \frac{r}{\cos(\theta)} - r) \tag{4b}$$

$$Total\ Area\ of\ tori = \sum_{i=1}^{n}(2 * \pi * R(i)) * (2 * \pi * r) \tag{4c}$$

$$Total\ Volume\ of\ tori = \sum_{i=1}^{n}(2 * \pi * R(i)) * (\pi * r^2) \tag{4d}$$

$$Total\ Mass = D\_g * total\ volume\ of\ tori + D\_f * total\ area\ of\ tori * t \tag{4e}$$

$$Packing\ Density = \frac{Payload\ mass}{L * (\pi * (D_N - 2 * r)^2)} \tag{5}$$

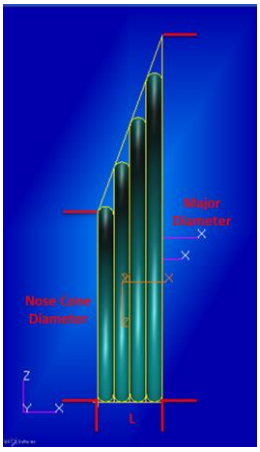

Figure 5: Side View of 100% Shifted HIAD

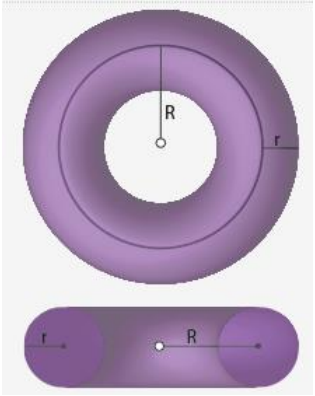

Figure 6: Geometry of a Torus [27]

	Viking	MER	MSL
Entry Mass (kg)	992	~830	3600
Aeroshell Diameter (m)	3.5	2.65	4.5
Packing Density (kg/m^3)	118.5	235.5	187
Ballistic Coefficient (kg/m^2)	64	94	142
L/D$_{max}$	0.18	0	0.24
Peak Heat Rate (W/cm^2)	26	44	136
3σ Error Ellipse Major Axis (km)	280	80	12.5
Landing Site Elevation (km MOLA)	-3.5	-1.4	1

Figure 7: Comparison of Previous Mars Robotic Mission Packing Densities [28]

Results were saved for analysis and used in further simulations. These results include D_N, D_0, θ, L, r, number of tori, inflatable structure total mass, fabric mass, and gas mass, location of each torus center in the XZ-plane, R, and required packing density. The objective function for each configuration was calculated

using Equation 3. A summary of the objective function results is shown in Table 4, indicating that both the packing density and objective function increase with increasing number of tori. From Figure 7, the packing densities for the previous Mars robotic missions vary between 120 $\left(\frac{kg}{m^3}\right)$ and 240 $\left(\frac{kg}{m^3}\right)$. For this asymmetric HIAD geometry, the design composed of 4 tori had a packing density of 135 $\left(\frac{kg}{m^3}\right)$. This density was assumed to be a reasonable upper limit. Therefore, the 4 tori design best satisfied the objective function subject to the packaging and tori manufacturing constraints.

Table 4: Objective Function and Packaging Density Results for 100% Shifted HIAD Designs Employing Different Number of Tori - All Designs Have a 9 (m) Diameter Nose Cone, 17.5 (m) Major Diameter and 70 Degree Cone Angle

Total # of tori	4	5	6	7	8	9	10	11	12	13	14	15
Torus radius (m)	0.39	0.31	0.26	0.22	0.19	0.17	0.15	0.14	0.13	0.12	0.11	0.10
Packing density $\left(\frac{kg}{m^3}\right)$	135	146	154	160	164	168	171	173	175	177	178	1790
f(# of tori)	1.27	1.31	1.36	1.42	1.47	1.53	1.59	1.65	1.71	1.77	1.84	1.90

The final design, as chosen based on the objective function in Equation 3, assumed that design simplicity was equally as important as the decelerator system mass. However, it is important to understand how that weighting affects the final design. A sensitivity analysis was performed by adjusting the weighting of each component in the objective function, as shown in Equation 6. A summary of the results is listed in Table 5, and shows that increasing the importance of design simplicity (m) had little effect on the objective function and did not change the resulting design because the design was already limited by the packaging constraint. On the other hand, increasing the system mass weighting (n) was able to shift the desired design to higher number of tori (corresponding to lower system mass) but only when weighted three times more important than design simplicity. This insight showed that the desired design (4 tori) was relatively insensitive to variations in objective function weighting.

$$f(\#\ of\ tori) = n * \frac{mass(i)}{max\ (mass)} + m * \frac{tori\ \#\ (i)}{max\ (tori\ \#)} \tag{6}$$

Table 5: Summary of Objective Function by Varying the Weighting Values

n	1	1	1	1	2	3	4	5
m	2	3	4	5	1	1	1	1
Min(f)	1.533	1.800	2.067	2.333	2.267	3.265	4.242	5.202
Total # of tori	4	4	4	4	4	5	5	6

B. Construction Method

A stacked tori method was chosen, as was utilized on the IRVE-3 test vehicle, to create the shifted shape. In the IRVE-3 test vehicle, the tori were stacked in a symmetric configuration, held in place with radial and pairing straps as shown in Figure 8. The tori in the chosen design can be stacked similarly, but instead of symmetrically, only one point on the tori will be stacked. This configuration is demonstrated in the side view of Figure 5.

The shifted configuration shown poses a problem with how the tori would be held together. In the previous configuration the straps solved this problem as all attachment points were equally spaced from one another. In the shifted configuration, the tori get further from each other around the circumference. This means that straps would have be differing lengths and shapes in order to meet the current requirements.

The developed solution is a concept called the FlexShell. The FlexShell incorporates the benefits of the straps without the complications that the straps pose. The FlexShell will be a continuous membrane of Kevlar that covers all of the HIAD tori. This layer will reside between the inflatable tori and the thermal protection system. The FlexShell will be cut such that it forms an outer shell to the desired shifted HIAD shape. This shell will then cover the inflated tori and they will have continuous attachment to the FlexShell, effectively distributing any aerodynamic forces as well as holding the tori into the desired shifted shape.

In order to create a stronger FlexShell, one large sheet of Kevlar will be used with a single seam connecting the edges to create the three dimensional shape. This seam will run along the vertical part of the HIAD, next to the tori that are tangent to each other and the cylindrical payload fairing.

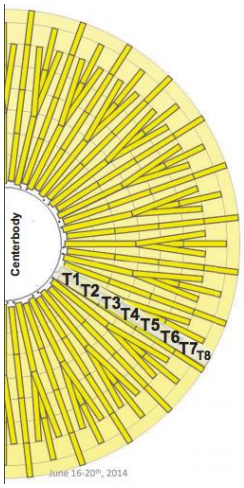

Figure 8: IRVE-3 Radial Strap Diagram [29]

Packing the tori and FlexShell will require a different packing configuration than the symmetric HIAD. In this new configuration, the inflatable structure will be packed around the cylindrical payload fairing rather than around the nose of the vehicle. This will require a secondary cloth cover that keeps the tori and FlexShell compacted, also protecting it from micrometer and orbital debris damage. This cloth cover will be jettisoned prior to HIAD inflation.

C. Structural Analysis

Structural analysis was used to validate the integrity of the chosen design shape, being described via two metrics: maximum deflection and maximum stress. The Patran/Nastran software package was used for the analysis. The first step was to import the geometric information required to construct the model from the mass calculations. The center location of each torus and their major radius were used to construct each torus model. Two lines were then created along *L* and the longest side of the HIAD, as shown in Figure 5. Both of these lines lay tangent to each of the tori. The FlexShell wrap was created based on these two lines and two circular curves defined by the rigid nose cone and the major diameter. Once the geometry was created, the material properties were defined and assigned to their corresponding components. Since it was assumed that both the FlexShell and the tori were made of Kevlar, only one material property was required for this model, with isotropic material properties shown in Table 6 [25]. Following the material definition, the next step was to mesh the geometry. The mesh size can be chosen based on the size of the overall structure as well as individual components. In this model, a mesh size of 0.2 (m) was chosen. Boundary conditions were then applied to the model. Since the first torus was assumed to be fixed to the rigid nose cone, fixed boundary conditions were applied to all the nodes on the first torus that were in contact with the nose cone. An additional fixed boundary condition was also applied to simulate the fact that all of the tori along the short side (*L*) were attached to the payload cylinder. There were two loading conditions applied to the model: internal inflation pressure and external dynamic pressure. An internal inflation pressure of 15 (psi) was applied to the interior of all tori and the external dynamic pressure was applied to the outside of the flexible wrap. The magnitude of external dynamic pressure corresponded to the maximum dynamic pressure obtained from the trajectory simulation. The finite element model was solved in Nastran and the results were imported back to Patran for post-processing.

Table 6: Kevlar Material Property

Elastic Modulus (Pa)	Poisson Ratio	Shear Modulus (Pa)	Density (kg/m^3)
3E9	0.36	1.1E9	1150

Due to difficulties with model convergence, cases were only run with an applied inflation load to the tori (no FlexShell or external loading). As shown in Figure 15, the maximum displacement occurred on the largest torus with a maximum value of 0.573m. This displacement corresponded to 3% of the 17.5 (m) HIAD major diameter. In addition, the constraint forces were calculated as shown in Figure 16. The stress resulted from the imposed fixed boundary conditions along the shortest side (L) of the HIAD. The Von Mises stress results are also included, seen in Figure 17. The figures from this section can be found in the appendix.

This model demonstrated the first steps towards developing a full finite element analysis of the inflatable aeroshell, which will be performed prior to the presentation milestone. The full model will expand on the results presented here while including the FlexShell and external loading. Both the overall deflection and resulting stresses will be analyzed to better understand the structural performance of the proposed design.

Preliminary structural results were estimated for this study using modified versions of the structural equations found in the IAD dimensionless mass estimation study [30]. In the derivation of the IAD mass, four different structural capabilities were defined and derived: inflatable structure resistance to external loading, inflatable torus fabric strength, gore fabric strength, and radial strap strength. The equations for these parameters were derived assuming an axisymmetric inflatable aeroshell. As a result, it was required to re-derive these equations in order for them to be applicable to the asymmetric shifted HIAD configuration proposed by this project.

The inflatable structure resistance to external loading calculations estimate the minimum inflation pressure required to ensure zero circumferential stress in the membrane under maximum loading [31]. The calculations use the principal of virtual work to equate the work done by an external aerodynamic load (F_A) through a structural displacement (δ) and the volume change (dV) of inflation gas multiplied by the inflation pressure (P) as a result of a cone angle deflection. The principal of virtual work is formulated via Equation 7. The following calculations for the asymmetric vehicle differed from the original calculations. The structural displacement (δ) can be determined from θ and D_0 as in Equation 8. The gas volume of the decelerator can also be estimated by relating the asymmetric design to its equivalent symmetric design. The shifted HIAD geometry is achieved by displacing successive tori so that they are tangent along L. These tori can also be re-arranged to form a symmetric shape, which because it is composed of the same inflatable members, will have the same inflated volume. The relationship between the asymmetric (θ) and symmetric (θ_S) cone angles is described in Equation 9 and the inflated volume is calculated in Equation 10. These parameters can then be used in the virtual work relation (Equation 1) to solve for the required inflation pressure, as seen in Equation 11. In this equation the dynamic load is taken to be the drag load qC_DA_{ref} from the dynamic pressure (q), drag coefficient (C_D), and reference area (A_{ref}).

$$F_A \partial\delta = -P\partial V \tag{7}$$

$$\delta = \frac{2D_0}{3tan\,(\theta)} \tag{8}$$

$$\theta_S = tan^{-1}\left(\frac{tan\,(\theta)}{2}\right) \tag{9}$$

$$V = \frac{\pi {D_0}^2 r}{4sin\,(\theta_S)} \tag{10}$$

$$P_{min} = \frac{2qC_DA_{ref}sin^2\,(\theta_2)(3cos\,(2\theta)+5\,)}{3\pi D_0 r cos\,(\theta_2)} \tag{11}$$

For the design parameters from the aerodynamic and mass analyses, the required P_{min} was 24 (psi). The inflatable torus fabric strength calculations were not re-derived in this study because testing of inflatable tori has been conducted to pressures exceeding the required minimum pressure. The gore fabric strength calculations were also not considered. In the original derivation, the gore was intended to support the local surface pressure while radial straps were used to support the decelerative loading. In the current proposed design, the FlexShell is intended to satisfy both requirements. Of the two conditions, it is expected that the

decelerative loading will be the dominant constraint. Therefore, the FlexShell structural performance is assessed via the radial strap relations from the original paper.

The following calculations for the asymmetric vehicle differed from the original calculations. The maximum stress on flex cover will occur along the attachment to the rigid nosecone because it has the smallest cross-sectional area and experiences the full load. The stress (σ) in this region is described by Equation 12, where θ_H is the local FlexShell angle and dl is the infinitesimal circumference. The local FlexShell angle can be described by Equation 13, where ϕ is an angle centered in the middle of the largest torus with $\phi = 0$ pointing towards the shortest edge. The circumference is therefore $dl = \frac{D_N}{2} d\phi$ and the stress can be described via Equation 14, with F(x|m) being the elliptic integral of the first kind with parameter $m = k^2$.

$$\sigma = \frac{F_{Drag}}{\int \cos(\theta_H) t \, \partial l} \tag{12}$$

$$tan\,(\theta_H) = \frac{\sqrt{1-cos\,(\phi)}\,tan\,(\theta)}{\sqrt{2}} \tag{13}$$

$$\sigma = \frac{q C_D A_{ref}}{D_N\, t\, F(-tan^2\,(\theta))} \tag{14}$$

Using the specified design parameters resulted in a stress of 0.047 (GPa). Therefore, the tensile stress in the FlexShell was less than the FlexShell tensile strength (Kevlar, $\sigma_Y = 3$ (GPa)), which demonstrated that the FlexShell has the potential to support full aerodynamic loading during entry. Alternatively, this relation can also be used to determine the maximum sustainable dynamic pressure loading. Assuming that the FlexShell has a yield strength of 3 (GPa), the maximum possible loading for the proposed geometry is 706 (kPa). Overall, the structural analysis showed that the shifted HIAD design proposed in this study had sufficient structural strength. This will be further assessed with high fidelity finite element analysis prior to the presentation deadline.

D. Lift to Drag Modulation

The selected optimized geometry successfully achieves the maximum L/D requirement and the pitch static stability requirement. To fully satisfy the Big Idea Challenge goals, L/D must be modulated between 0.2 and 0.5. Two methods can be considered, including pitching L/D modulation and rolling lift vector shift.

1. Pitching L/D modulation

The magnitude of the L/D ratio can be modulated by bringing the CG closer to the cylindrical payload fairing centerline. Doing so, this configuration will trim at a lower angle-of-attack and reduce L/D. The range of L/D ratios achievable by this design are shown in Figure 9.

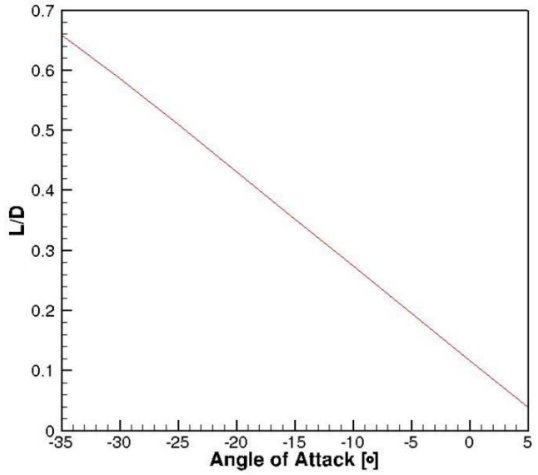

Figure 9: L/D vs. Angle of Attack

2. Bank Modulation Effect on Lift Vector Shift

The direction of the shifted HIAD configuration's lift vector can be controlled via bank angle modulation shown in Figure 10. In this manner, the vehicle is rotated around the axis parallel to the freestream velocity vector passing through the CG. Note that the orientation between the flow and the HIAD is the same as the bank angle changes. Relevant expressions are shown with Equations 15-17. For each vertical component of the lift vector L_V, the bank angle can be determined as shown in Table 7.

$$C_{L_V} = C_{L_V\ at\ no\ bank\ angle} \times cos\emptyset \quad (15)$$

$$C_D = C_{D\ at\ no\ bank\ angle} \quad (16)$$

$$L_V/D = 0.500 \times cos\emptyset \quad (17)$$

Table 7: Required Bank Angle for L_V/D Regimes

L_V/D	0.2	0.25	0.3	0.35	0.4	0.45	0.5
$\emptyset$[°]	66.42	60.00	53.13	45.57	36.87	25.84	0.00

Therefore, the shifted HIAD can modulate L_V/D from 0.2 to 0.5. A bank acceleration of 5 (°/s^2) was assumed to calculate the reaction control system (RCS) propellant required and maneuver time. As shown in Table 8, the lift vector shift system is considered to modulate from 0.5 to 0.2 in increments of 0.05. When the HIAD shifts from one bank angle to another, the bank acceleration is 5 (°/s^2) for the first half of the maneuver time and -5 (°/s^2) for the second half of the maneuver time. This method allows the desired bank angle to be achieved with a value of 0 (°/s) for banking angular velocity.

The estimation of total fuel mass necessary for bank angle modulation was performed and shown in Table 8. A Tri-gas Thruster [31] RCS system with an Isp of 221 (s) was chosen to generate the necessary moment to accomplish the banking lift vector shift. The moment of inertia of the HIAD about the centerline of the cylindrical payload fairing was calculated to be approximately 212,000 (kg·m^2), assuming that the total vehicle mass is 21 (metric tons) with even mass distribution inside its cylindrical shape. The moment calculations are performed assuming a RCS moment arm of 7.16 (m), indicating the RCS system is attached to the rigid payload fairing, equivalent to point H in Figure 1. As a result, the total mass of the necessary fuel is 1180 (kg) which is the sum of the necessary fuel of each shift.

Table 8: Fuel Mass Required for L_V/D Shifts

L_V/D Shift	0.45-0.50	0.40-0.45	0.35-0.40	0.30-0.35	0.25-0.30	0.2-0.25
Acceleration Δt (s)	2.273	1.486	1.319	1.230	1.172	1.133
Total time (s)	4.546	2.971	2.638	2.459	2.344	2.266
Total Req. Prop. Mass (kg)	311.51	203.52	180.75	168.50	160.62	155.27

3. Roll Stability

In either method above, it is necessary to achieve static stability about the roll axis at a bank angle of 0°. However, the shifted HIAD cannot meet this requirement because $C_{l_\emptyset} > 0.00$ at a bank angle of 0°, as shown in Figure 11. For static rolling stability to be achieved, the following two conditions must be met in Equation 18 and Equation 19:

$$C_l = 0.00 \quad (18)$$

$$C_{l_\emptyset} > 0.00 \quad (19)$$

Therefore, the vehicle is not stable about the rolling axis. Because the shifted HIAD flies at a roll angle of 0°, no device is needed to provide rolling control. However, during reentry there are perturbations that may cause the roll angle to deviate from its nominal 0°. Therefore, the estimation of total fuel mass necessary to control roll angle was performed. The Tri-gas Thruster RCS system [32] is used again to generate a counter rolling moment to resist roll angle deflections. The moment of inertia calculated in the *Bank Modulation Effect on Lift Vector Shift* section was used as the moment of inertia around the x-axis

here as well. The assumption was made that there must be adequate fuel to hold the HIAD within a roll angle of 2° during total EDL phase. The moment was calculated using the velocity and altitude as the maximum dynamic pressure condition in order to obtain a conservative estimate of the total fuel mass required. Moment calculations were performed assuming a RCS moment arm of 7.16 (m), indicating the RCS system is attached to the point H in Figure 1. Table 9 presents the inputs used in this estimation and the result shows that approximately 236 (kg) fuel is necessary.

Table 9: Inputs for Mass Estimation of Fuel

Altitude (km)	Velocity (km/s)	C_l at Ø = 2°	Rolling Moment at Ø = 2° (N m)	EDL duration (s)	Total fuel mass (kg)
30	4.5	0.000144	6097.2	600	235.76

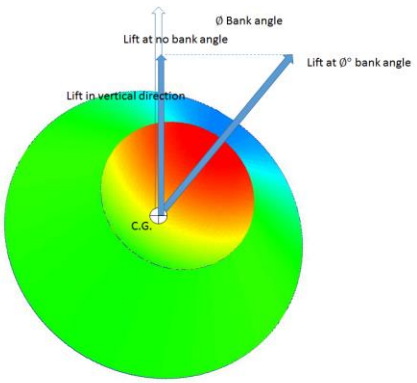

Figure 10: Banked Configuration of shifted HIAD (Left)

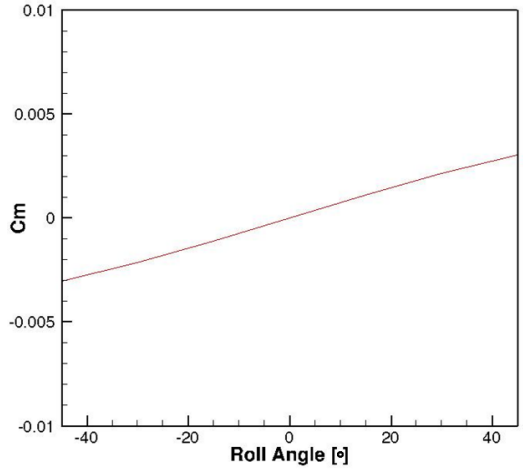

Figure 11: Rolling Moment Coefficient vs. Roll Angel at CG Location of (2.34, 0, -2.66) (Right)

E. Trajectory Flight Envelope

After the method of lift modulation had been determined, the team performed a trajectory analysis using a computer simulation written in Matlab. The Aeroassist Simulation (ASIM) was developed in the Space Systems Design Laboratory over many years and uses the first order approximation equations of entry to generate predicted entry trajectories. In this study, ASIM was configured to generate banked lifting trajectories in the Martian atmosphere using a MARSGRAM atmospheric model. Aerodynamic information obtained for the final shape was also incorporated into the trajectory simulation.

The previous section discusses in detail how the HIAD concept can generate a lift-to-drag ratio of 0.5 at a bank angle of 0° and a lift-to-drag ratio of 0.2 at a bank angle of 66.4°. The next analysis step was to determine the entry conditions (velocity and flight path angle at Mars entry interface). As a first-cut approximation, the team used the Mars Science Laboratory (MSL) entry conditions, which corresponds to an entry velocity of 6 (km/s) and an entry flight path angle of -15.2° relative to the local horizontal at a Mars entry interface altitude of 125 (km). The team assumed that the entry velocity was fixed and set out to find if the MSL flight path angle would be adequate for the mission at hand.

Figure 18 - Figure 21 show six resulting trajectories for the lift-to-drag ratio of 0.5 case at different flight path angles. One can see from Figure 18 that the most shallow flight path angle of -15.2° results in atmospheric skip out, which is undesirable. To prevent skip out, it is desirable to enter at a steeper flight path angle of -25°. For this steep trajectory, the resulting maximum dynamic pressure and maximum heat flux are approximately 13 (kPa) and 22.5 (W/cm^2), respectively. The structural analysis of the selected HIAD vehicle shows that it can withstand a maximum loading of 706 kPa and past thermal analysis shows that previous Flexible Thermal Protection System (FTPS) for HIADs can withstand a heat flux up to 50

(W/cm^2) [24]. Therefore, entering at a flight path angle of -25° is feasible from both structural and thermal standpoints and will be selected as the entry flight path angle for all trajectories.

The following analysis shows the flight envelope between the maximum and minimum lift-to-drag ration configurations. The entry conditions are assumed to be the same for all trajectories, which has been chosen to be an entry velocity of 6 (km/s) and an entry flight path angle of -25° relative to the local horizontal at a Mars entry interface altitude of 125 (km). The resulting trajectories for lift-to-drag ratio configurations of 0.5 and 0.2 are shown in Figure 22 through Figure 27. It is important to note that the lift-to-drag ratio of 0.2 is achieved by holding a bank angle of 66.4°, which produces a crossrange component shown in Figure 27. This crossrange component can be accounted for before entry or it can be mitigated during flight if the vehicle holds a bank angle of -66.4° for a significant amount of time. Overall, this trajectory analysis confirms that the desired range of entry trajectories are feasible and favorable for landing high-mass payloads on the surface of Mars.

F. Extensibility to Large Scale Operation

This investigation has performed an in-depth feasibility study of a novel HIAD concept. The goal of the NASA Big Idea Challenge is to use a proposed concept to eventually land high-mass payloads on the surface of Mars. As stated, payloads of approximately 20 (metric tons) may be landed by HIAD concepts with diameters of approximately 20 (m). Most importantly, the proposed vehicle must be scalable and extensible to this high-mass operation mode.

The team decided to consider a full-scale vehicle from the beginning of the analysis in order to give an adequate evaluation of feasibility. The payload has been assumed to be approximately 20 (metric tons) and asymmetric HIAD concepts with diameters between 15 (m) and 20 (m) have been considered. The final selected concept has a major diameter of 17.5 (m). Because our studies have shown that our final selected concept is feasible and meets the specified design constraints, the team is confident that it is extensible to large-scale and full-scale operation. To confirm that HIAD diameters larger than 20 (m) are feasible, the analyst would need to re-run the presented analysis for larger diameter HIADs.

IV. Systems Analysis of Requirements, Including Identification of Challenge and TRL of Mission-Enabling Technologies

A. Systems Analysis of Requirements

The following design requirements are the guidelines for the HIAD taken directly from the problem statement:

Design Requirements
1. HIAD concept shall be suitable for payloads up to 20 (metric tons).
2. HIAD concept shall provide modulated L/D ratio of 0.2 to 0.5 during hypersonic entry.
3. HIAD concept shall be aerodynamically stable between 6.5 (km/s) to 0.6 (km/s).
4. HIAD concept shall fit in payload fairing of Space Launch System.

All system level requirements generated during this design process trace directly to these design requirements. The system under consideration is the HIAD with two subsystems identified, the inflatable structure and the RCS thrusters, which have requirements based on the selected configuration. Table 10 lists the system level requirements for the design, and shows which system requirements satisfy each design requirement. Table 12 shows the subsystem level requirements and the traceability to the system level requirements.

Table 10: System Level Requirements

Req. No.	System	System Level Requirement	Traceability
1.1	HIAD	Shall have thermal protection system to withstand thermal loads over entry trajectory.	1

1.2	HIAD	Shall have scalable major diameter of 15 to 20 m.	1
1.3	HIAD	Shall provide lift at trim condition.	2, 3
1.4	HIAD	Shall have a reaction control system to modulate lift.	2
1.5	HIAD	Rigid aeroshell shall be less than 9 m in diameter.	4
1.6	HIAD	Inflatable structure shall be able to be packed to fit within payload fairing.	4

B. Identification of Challenges

A major challenge in developing a new technology such as the FlexShell is how it would attach to the tori. The design proposed is a continuous stitch that connects the FlexShell and the tori at the point where they are tangent to each other. This method will effectively transfer the stresses between the tori. Additionally, this method will ensure that the tori do not translate with respect to one another, changing their position from the desired configuration. Additionally, no data is available to compare the relative importance of required system mass and design simplicity, no data is available on the reasonable manufacturing capabilities for torus, and it is unclear if complexity scales linearly with number of tori.

C. TRL of Mission-Enabling Technologies

The overall TRL of the system is 2, this is because the lowest TRL of all the technology subsystems is TRL 2. The asymmetric HIAD that is proposed has three main technology subsystems: the inflatable structure, the packing system, and the RCS to modulate the lift. The inflatable tori and their attachment to the center body are at a TRL of 7 because they have been tested in a space environment, as seen in the successful test flight of IRVE-3 [33]. The inflatable technology has undergone structural testing as well, ensuring that stacked tori can withstand static loads [34]. However, the shifted configuration that we are utilizing is only at a TRL of 3, because there have only been analytical studies done on it as a proof-of-concept [17]. The FlexShell technology that we are proposing has the lowest TRL of 2, because this is only a concept and has had no studies performed yet.

The RCS thrusters and tank are given the highest TRL of 7. Both numerical and experimental analysis has been done on the effect of RCS thrusters on hypersonic reentry. Additionally, an RCS was flown at Mars as on MSL, however MLS did not utilize a HIAD for entry [35]. Table 11 summarizes the TRLs of the HIAD concept systems and subsystems.

Table 11: TRLs of HIAD Concept Systems and Subsystems

Technology System	TRL
Asymmetric HIAD	2
1. Inflatable Structure	3
1.1 Tori	3
1.1.1 Asymmetric Stacked Configuration	3
1.1.2 Inflatable tori	7
1.1.3 Attachment to Rigid Body	7
1.2 FlexShell	2
1.2.1 Construction of Kevlar Sheet	2
1.2.2 Attachment to tori	2
2. RCS	7
2.1 Thrusters	7
2.2 Propellant Tanks	7

V. Evidence of Credible and Implementable Project Plan, Cost, and Schedule

The ultimate goal of this project will be to create a robust HIAD system certified for implementation on future missions by the end of 2019, and to expand HIAD technology to the point where it can be implemented in Mars surface missions from 2024 onwards. The program will consist of 3 phases: concept studies and vehicle design, extensive ground testing, and a flight test to certify the system. The concept studies are to be conducted throughout 2016. The aim of these studies will be to evaluate potential HIAD

designs we have outlined and select one design for further development. The team will use computer simulations, spacecraft modeling, and cost and simplicity evaluations to decide upon the ideal configuration for the flight vehicle. At this point, the HIAD system will be able to compete for future funding as a part of the Space Technology Mission Directorate. Given how essential this technology is for future robotic and piloted missions, continued system development will be a high priority.

A. Project Plan, Schedule, and Cost Estimate

If selected for further funding, the HIAD project will construct a ground test article to evaluate the selected design using actual hardware. It will be 5 (m) in diameter and incorporate lessons learned from the IRVE program, a decade of research and development projects, and the concept studies already carried out by this program. The test article will carry a set of avionics and an extensive suite of sensors. Wind tunnel tests will validate the theoretical performance of the HIAD in a real-world environment. Testing at a NASA vacuum chamber will test the inflation and operation of the spacecraft in a relevant operational environment. The avionics testing will confirm that the spacecraft systems work together in unison.

If the final HIAD design shows promise, it will be tested in flight to provide a final verification of system capabilities. The flight test article will have the same configuration as the previously evaluated ground test vehicle, and incorporate modifications based on the extensive testing program. It will be carried to orbit on a sounding rocket and inflated prior to the vehicle's entry into the atmosphere. The test article will fly a reentry profile, being exposed to a higher heating environment than experienced by the IRVE series. The test vehicle will be recovered for analysis of the collected engineering data. By the end of 2019, the analysis of the collected data will be complete, and the HIAD will be certified for flight on future missions.

Assuming the success of the flight test program, the next steps for the HIAD project in the early 2020s will be to scale up and implement the design on future missions with the aim for use of a HIAD on a notional 2024 Mars lander that will be a precursor for human missions. An in depth schedule including proposed reviews has been included in Figure 29.

A system level cost estimate has been performed on the HIAD project, and a budget timeline is presented in Figure 28. We estimate a total cost of $80 million for the entire program, from conception to the completion of the Mars precursor mission in 2025. We will need $20,000 for concept studies and system tests lasting until the end of 2016. We estimate that the major components of the budget will consist of salaries, HIAD vehicles material and construction cost, and the facilities for testing them. The most significant costs coming from the personnel and launch costs. An estimated cost breakdown can be found in the appendix. By the end of 2025, the HIAD project will have developed a certified system with a TRL on par with that of a rigid heat shield available for use on future missions, including rocket reuse, ISS cargo return, sample returns from the outer solar system, and both robotic and crewed missions to Mars.

VI. Next Steps for Analysis on Proposed HIAD Concept

A. Next Steps for Current Asymmetric HIAD Design

The team plans to extend analysis in many directions to improve the performance and feasibility of the proposed concept. The HIAD geometry selection process can consider shapes that target positioning the vehicle's CG along the centerline of the cylindrical payload fairing. The main benefit would be reduced packing constraints on the payload and full utilization of payload fairing internal volume. Geometry selection with consideration of the CG location is valuable because its desirable to have the CG located along the centerline of the cylindrical payload fairing. Figure 12 shows how the pitching moment coefficient changes with angle-of-attack if the CG is fixed at (x, y, z) = (2.34 0, 0) (along the centerline of the cylindrical payload fairing). By using trends seen in Figure 12, an L/D of over 0.5 can be achieved with static stability about the pitch axis at an angle-of-attack of -62.5°, which is shown in Figure 13 and Figure 14.

An estimation of the propellant mass required for two 180° roll reversals during the nominal entry, descent, and landing sequence for the L/D = 0.5 configuration will also be necessary. Future mass modeling will incorporate a more detailed mass break down and different objective functions that can be reevaluated based on the relative impacts of required system mass and design simplicity. Further structural analysis, including high fidelity finite element analysis, will be performed and validated with further material testing and subscale model testing.

The development of the FlexShell will be an ongoing process. The team is dedicated to designing the most effective method of creating the three dimensional shape of the 100% shifted HIAD. The FlexShell is comprised of a continuous, single-sheet of high-density Kevlar. As a result, it is likely to contribute significantly to the inflatable structure mass, which can be considered in a more comprehensive objective function shown in Equation 3. Additionally, more development is necessary to find the most effective method of stitching the FlexShell to the tori. Examining the stitching pattern, stitching material, and attachment point locations are all considerations for the next round of analysis.

Further trajectory analysis is necessary to ensure that peak heating and dynamic pressures to not exceed vehicle limitations. A single event drag modulation will also be compared to the lift modulation trajectory to determine if similar trajectories can be produced with both methods.

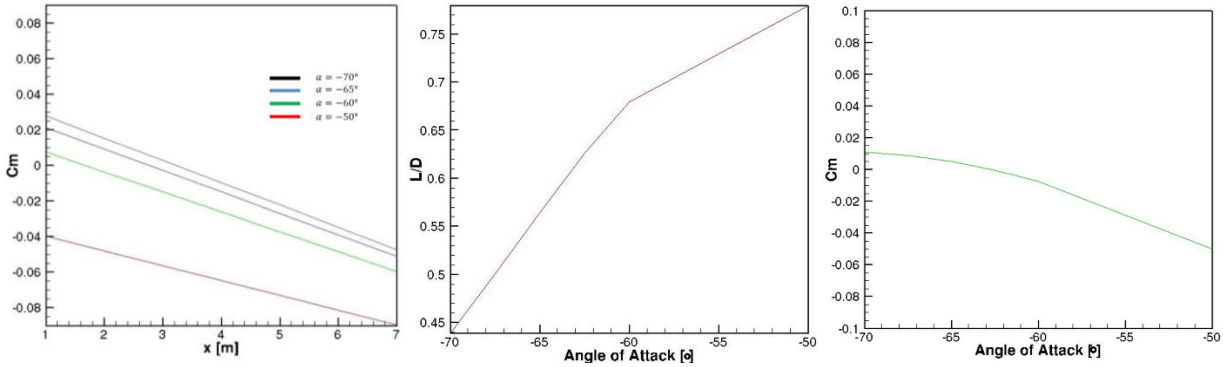

Figure 12: Pitching Moment Coefficient (C_m) with Potential CG Locations (Left)
Figure 13: L/D vs. Angle-of-Attack (Center)
Figure 14: Pitching Moment Coefficient (C_m) at CG Location (2.34, 0, 0) (Right)

VII. Conclusion

This technical paper has presented a new HIAD concept geometry designed to achieve the Big Idea Challenge design constraints while minimizing the required trim angle of attack to achieve an L/D of 0.5. A novel "100% shifted HIAD" stacked tori configuration was identified, analyzed, and shown to be an attractive and feasible design. This geometry satisfies the pitching static stability requirement in the desired flight regime. Through the use of bank angle modulation, the proposed HIAD design has the capability to modulate L/D from 0.5 to 0.2. After performing a study to balance HIAD mass and complexity for the final HIAD configuration, it was found that four tori most effectively minimize the overall objective function. A sensitivity analysis was also performed to determine the effects of weighting different combinations of final design parameters. Results show that system complexity weighting has little effect on the objective function due to external constraints, while the system mass weighting has a large effect on selection of final design parameters. The presented structural analysis used two approaches to evaluate the structural performance of the chosen configuration. Finite element analysis showed that the tori can withstand inflation loading of 15 (psi). A novel aeroshell system, called the FlexShell, covers the external surfaces of all tori to maintain the desired geometry and distribute structural loads evenly. Analytic approximations showed the HIAD to have sufficient resistance to deflection and demonstrate that the FlexShell can withstand the maximum aerodynamic loading obtained from trajectory simulations. A detailed trajectory analysis determined that the expected values of peak dynamic pressure and peak heating are can be withstood by the vehicle's structural components and Flexible Thermal Protection System (FTPS), respectively. Finally, a high level systems analysis was performed to establish the requirements of the HIAD technology system and to ensure the schedule and cost estimates are feasible.

Appendix

Nomenclature

A	=	amplitude of oscillation
a	=	cylinder diameter
α	=	angle of attack
β	=	bank angle
C_p	=	pressure coefficient
Cx	=	force coefficient in the x direction
Cy	=	force coefficient in the y direction
C_m	=	Coefficient of Pitching Moment
C_l	=	Coefficient of Rolling Moment
ϕ	=	roll angle
V_∞	=	free stream velocity

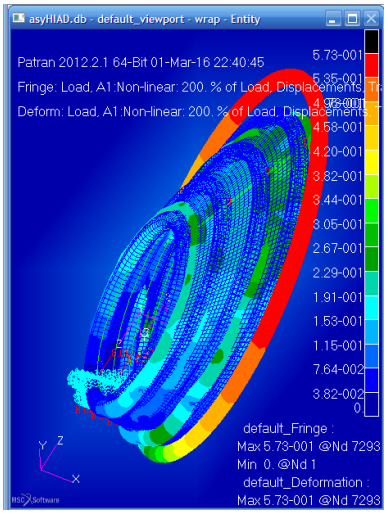

Figure 15: Displacement Result

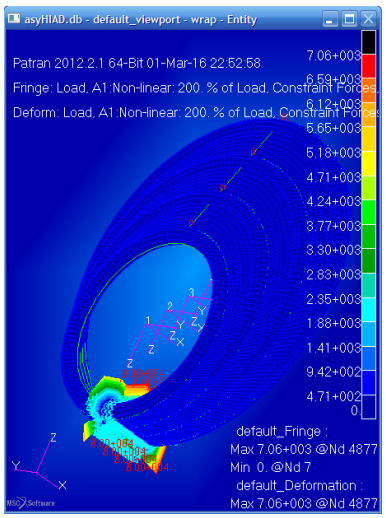

Figure 16: Constraint Force Result

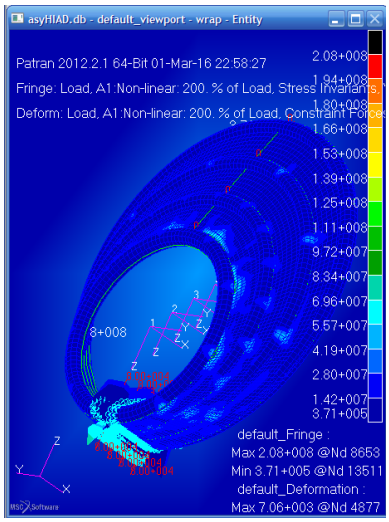

Figure 17: Von Mises Results

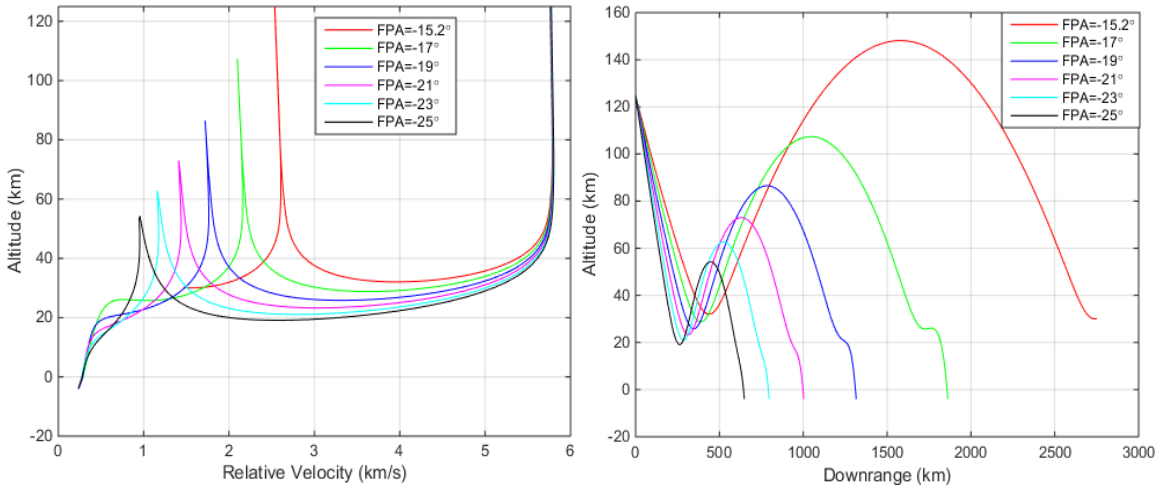

Figure 18: Altitude vs. Relative Velocity for Trajectories of Varying Flight Path Angles (Left)

Figure 19: Altitude vs. Downrange for Trajectories of Varying Flight Path Angles (Right)

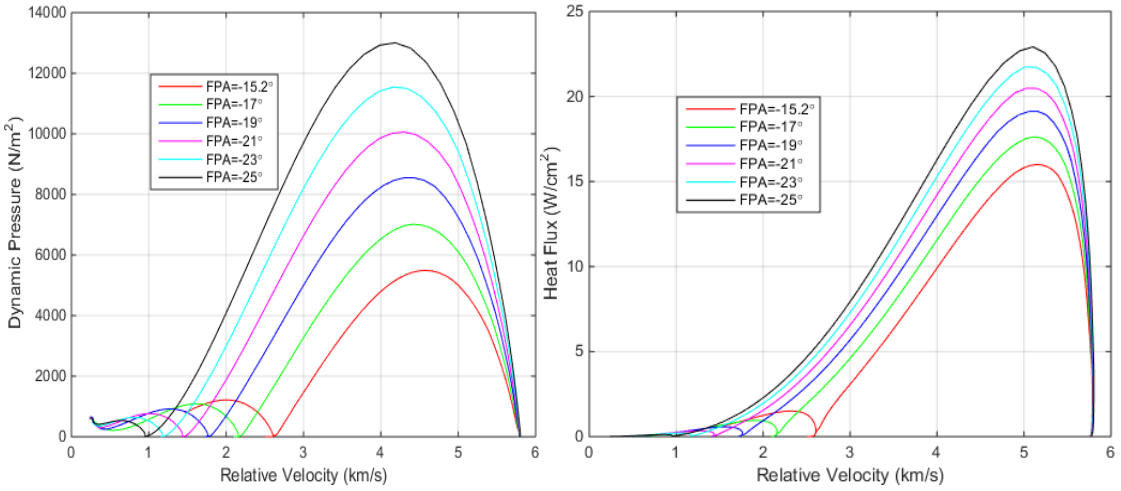

Figure 20: Dyn. Press. vs. Rel. Vel. for Trajectories of Varying Flight Path Angles (Left)
Figure 21: Heat Flux vs. Rel. Vel. for Trajectories of Varying Flight Path Angles (Right)

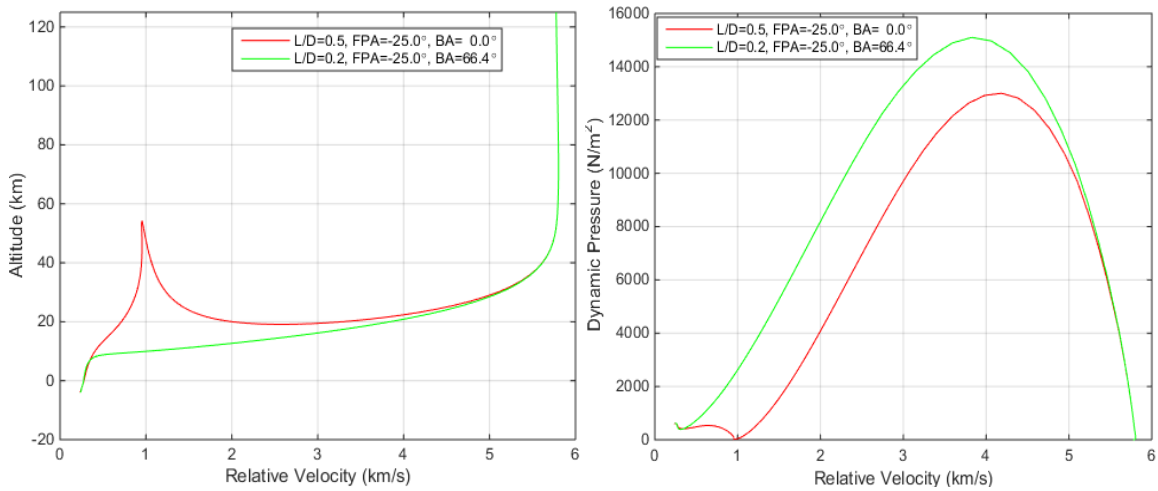

Figure 22: Altitude vs. Relative Velocity for Flight Envelope (Left)
Figure 23: Dynamic Pressure vs. Relative Velocity for Flight Envelope (Right)

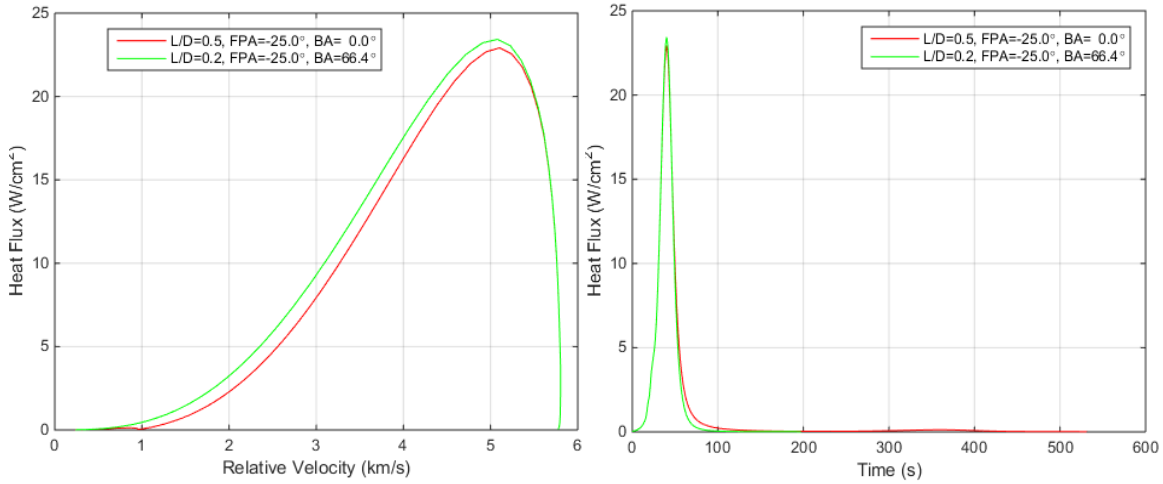

Figure 24: Heat Flux vs. Relative Velocity for Flight Envelope (Left)
Figure 25: Heat Flux vs. Time for Flight Envelope (Right)

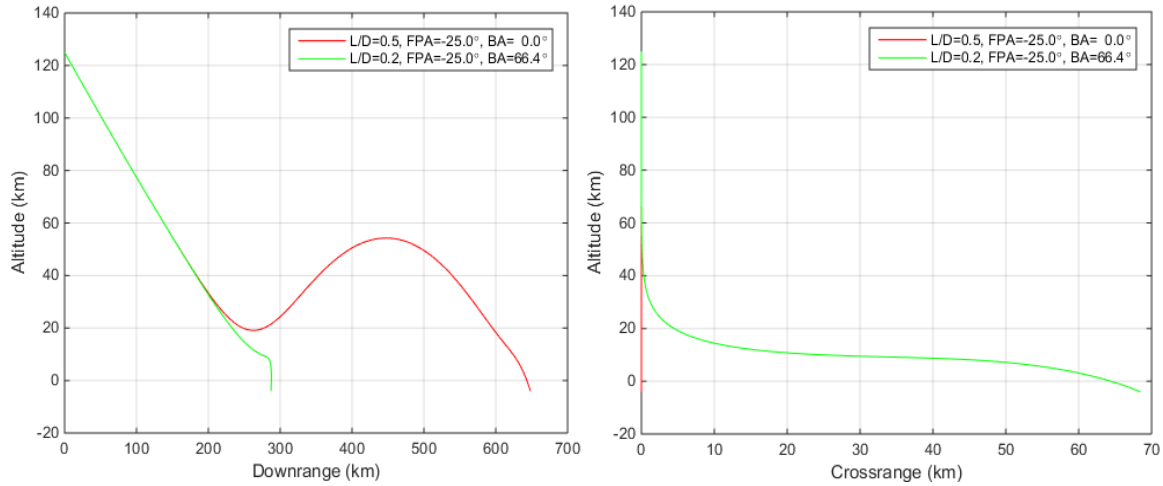

Figure 26: Altitude vs. Downrange for Flight Envelope (Left)
Figure 27: Altitude vs. Crossrange for Flight Envelope (Right)

Table 12: Subsystem Level Requirements

Req. No.	Subsystem	Subsystem Level Requirement	Traceability
1.1.1	Inflatable Structure	The inflatable structure shall be made up of tori of increasing major diameter to minimize mass and complexity.	1.2
1.1.2	Inflatable Structure	The inflatable structural shall be covered by flexible TPS and have a rigid heat shield for the center body and nose.	1.1, 1.5
1.1.3	Inflatable Structure	The inflatable structural shall be constructed to create a 100% shifted asymmetric shape.	1.2
1.1.4	Inflatable Structure	The inflatable structure shall be supported to provide structural stability and allow for HIAD to maintain shape during entry.	1.3

1.1.5	Inflatable Structure	The deflated inflatable structure shall be able to be compacted to fit within the payload fairing of the SLS.	1.6
1.2.1	RCS	Shall be able to control the rolling moment during entry.	1.4
1.2.2	RCS	The system shall contain tanks to hold fuel for RCS.	1.4
1.2.3	RCS	The RCS shall be able to provide control for X s during entry.	1.4
1.2.4	RCS	The RCS shall be able to roll the vehicle at a rate of 20 (deg/s) and an angular acceleration of 5 (deg/s^2).	1.4

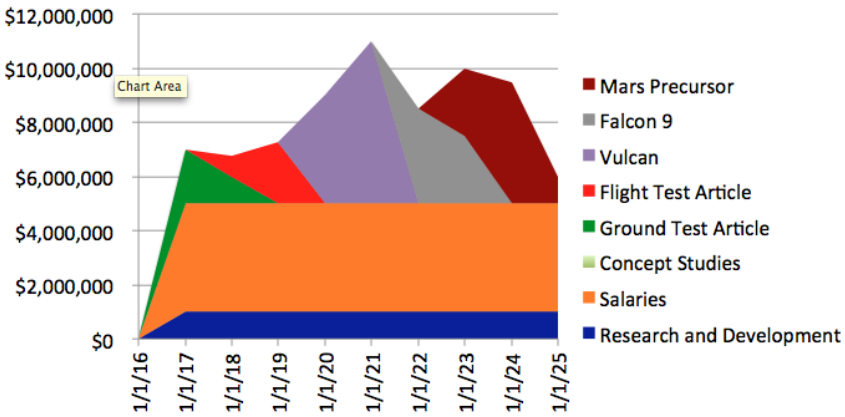

Figure 28: HIAD Project Budget 2016 - 2025

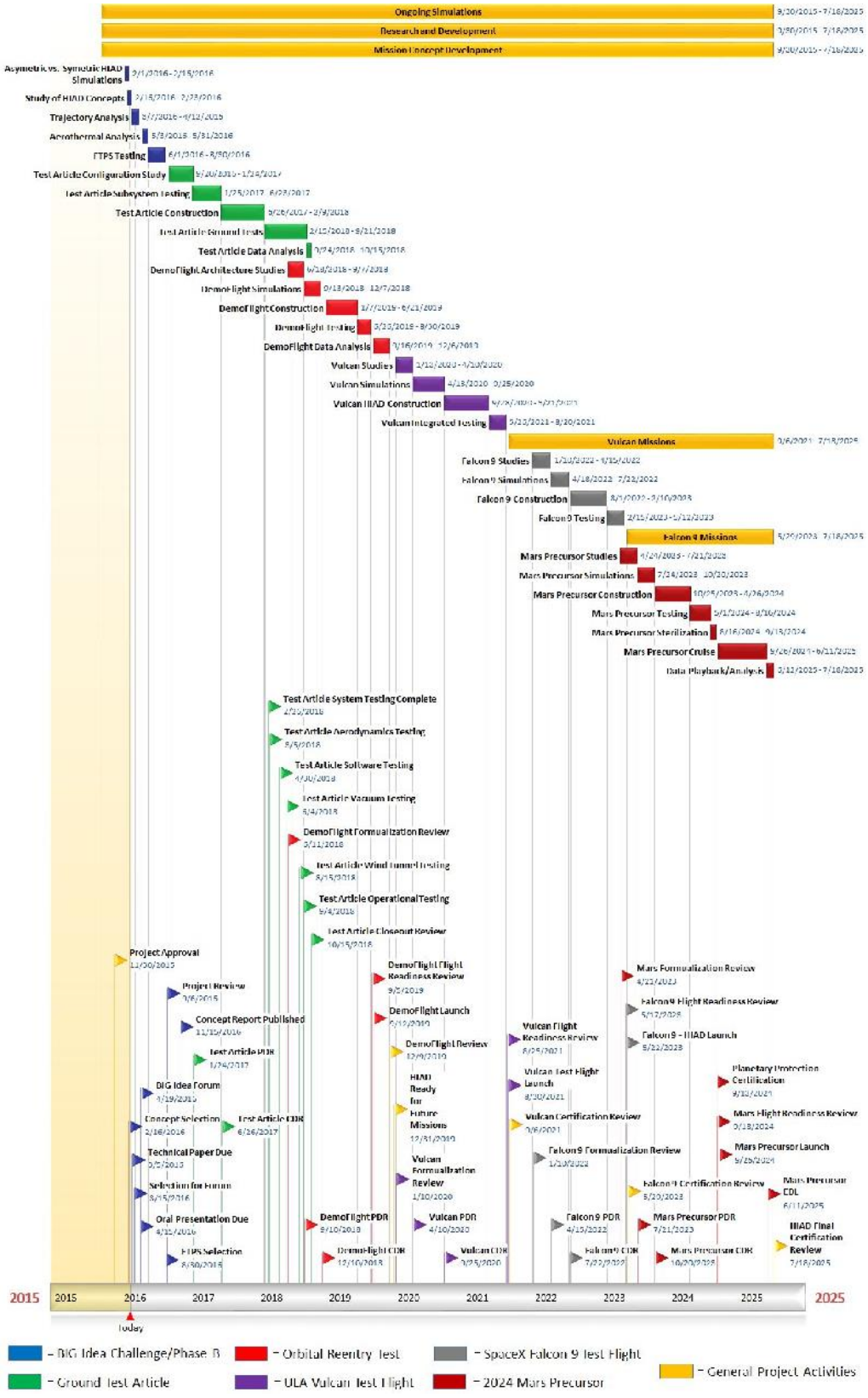

Figure 29: HIAD Project Schedule 2016 - 2025

Acknowledgments

The authors thank Dr. Robert Braun and Dr. Brandon Sforzo for their effective guidance and invaluable assistance completing this investigation. Additionally, the authors are grateful for all those participating in the HIAD research and development effort. Thank you for making this research possible and thank you for considering our proposal.

References

[1] Braun, R. D., and Manning, R. M., "Mars Exploration Entry, Descent, and Landing Challenges," Journal of Spacecraft and Rockets, Vol. 44, No. 2, March–April 2007, pp. 310–323. doi:10.2514/1.25116
[2] D. W. Way, R. W. Powell, A. Chen, A. D. Stelzner, A. M. San Martin, P. D. Burkhart, and G. F. Mendeck, "Mars Science Laboratory: Entry, Descent, and Landing System Performance," IEEE Aerospace Conference, 2006.
[3] Adler, M. et al, "Draft Entry, Descent, and Landing Roadmap: Technology Area 09," NASA, November 2010.
[4] Dwyer-Cianciolo, Alicia M., et al. "Entry, Descent and Landing Systems Analysis Study: Phase 1 Report." (2010).
[5] Ivanon, M. C., et al, "Entry, Descent, and Landing Systems Analysis Study: Phase 2 Report on Mars Science Laboratory Improvement," NASA/TM-2011-216988, July 2011.
[6] Steinfeldt, B. A., et al, "High Mass Mars Entry, Descent, and Landing Architecture Assessment," AIAA 2009-6684, AIAA Space 2009 Conference and Exposition, Pasadena, CA, September 2009.
[7] Drake, B. G. (Editor), "Human Exploration of Mars Design Reference Architecture 5.0," NASA/SP-2009-566, July 2009.
[8] Andrews, D. G., Cannon, J. H., Lund, E. A., Watry, K. E., "High Mass Mars Entry System: Architecture Design and Technology Development Roadmap," NASA/CR-2009-NNL08AA35C, September 2009.
[9] Smith, B. P., Tanner, C. L., Mahzari, M., Clark, I. G. Braun, R. D., and Cheatwood, F. M., "A Historical Review of Inflatable Aerodynamic Decelerator Technology Development," IEEEAC 1267, 2010 IEEE Aerospace Conference, Big Sky, MT, March 2010.
[10] Stephen J. Hughes, Robert A. Dillman, Brett R. Starr, Ryan A. Stephan, Michael C. Lindell, Charles J. Player, and F. McNeil Cheatwood: "Inflatable Re-entry Vehicle Experiment (IRVE) Design Overview'', 18th AIAA Aerodynamic Decelerator Systems Technology Conference and Seminar, Munich, Germany, May 24-26, 2005.
[11] Michael C. Lindell, Stephen J. Hughes, Megan Dixon, and Cliff E. Willey, "Structural Analysis and Testing of the Inflatable Re-entry Vehicle Experiment (IRVE)", AIAA-2006-1699
[12] Starr, B. R., Bose, D. M., Thornblom, M., and Kilcoyne, D. "Inflatable Reentry Vehicle Experiment Flight Performance Simulations," 53rd JANNAF Propulsion Meeting, Monterey, CA, Dec. 5-8, 2005.
[13] Stephen J. Hughes, Joanne S. Ware, Joseph A. Del Corso, and Rafael A. Lugo "Deployable Aeroshell Flexible Thermal Protection System Testing", 20th AIAA Aerodynamic Decelerator Systems Conference, May 2009.
[14] Stephen A. O'Keefe and David M. Bose, "IRVE-II Post-Flight Trajectory Reconstruction", AIAA-2010-7515 AIAA Atmospheric Flight Mechanics Conference, Toronto, Ontario, Aug. 2-5, 2010.
[15] Robert A. Dillman, Stephen J. Hughes, Richard J. Bodkin, David M. Bose, Joseph Del Corso, and F. McNeil Cheatwood: "Flight Performance of the Inflatable Reentry Vehicle Experiment II", 7th International Planetary Probe Workshop, Barcelona, Spain, June 14–18, 2010.
[16] O'Keefe, S. A., Bose, D. M., "IRVE-II Post-Flight Trajectory Reconstruction," AIAA Atmospheric Flight Mechanics Conference, AIAA Paper 2010-7515, 200914 O'Keefe, S. A., Bose, D. M., "IRVE-II Post-Flight Trajectory Reconstruction," AIAA Atmospheric Flight Mechanics Conference, AIAA Paper 2010-7515, 2009.

[17] Harper, Braun, "Asymmetrically Stacked Tori Hypersonic Inflatable Aerodynamic Decelerator Design Study for Mars Entry", AIAA Atmospheric Flight Mechanics Conference. National Harbor, MD 2014.
[18] Brooke P. Harper, Dr. Robert D. Braun, "Preliminary Design Study of Asymmetric Hypersonic Inflatable Aerodynamic Decelerators for Mars Entry"
[19] Mars Atmosphere Model - Metric Units – NASA Website URL: https://www.grc.nasa.gov/www/k-12/airplane/atmosmrm.html
[20] Anderson, J. D. J., "Hypersonic and High Temperature Gas Dynamics", McGraw-Hill, New York, 1989.
[21] Mars Atmosphere Model - Metric Units – NASA Website URL: https://www.grc.nasa.gov/www/k-12/airplane/atmosmrm.html
[22] Mars Fact Sheet –NASA Website URL:
http://nssdc.gsfc.nasa.gov/planetary/factsheet/marsfact.htmlNASA mars air
[23] Myers, R. H., Montgomery, D. C., Anderson-Cook, C. M., "Response Surface Methodology: Process and Product Optimization Using Designed Experiments," 3rd Edition, Wiley.
[24] Hughes, S. J., Cheatwood, F. M., Dillman, R. A., Wright, H. S., DelCorso, J. A., and Calomino, A. M., "Hypersonic Inflatable Aerodynamic Decelerator (HIAD) Technology Development Overview," 21st AIAA Aerodynamic Decelerator Systems Technology Conference and Seminar, Dublin, Paper 2011-2524, May 2011.
[25] "Technical Guide – Kevlar – Aramid Fiber", DuPont, 2016. URL: http://www.dupont.com/content/dam/dupont/products-and-services/fabrics-fibers-and-nonwovens/fibers/documents/Kevlar_Technical_Guide.pdf
[26] Cassell, A. M, Swanson, G. T., Johnson, R. K., Hughes, S. J., and Cheatwood, F. M., "Overview of the Hypersonic Inflatable Aerodynamic Decelerator Large Article Ground Test Campaign," AIAA 2011-2569, 21st AIAA Aerodynamic Decelerator Systems Technology Conference, and Seminar, May 2011.
[27] "Three-Dimensional Shapes: Polyhedrons, Curved Solids and Surface Area", SkillsYouNeed.com. URL: http://www.skillsyouneed.com/num/3d-shapes.html
[28] Ashley M. Korzun, Gregory F. Dubos, Curtis K. Iwata, "A Concept For The Entry, Descent, And Landing of High-Mass Payloads at Mars", URL: http://www.ssdl.gatech.edu/papers/conferencePapers/IAC-2008-D2.3.9.pdf
[29] Lyle, K.H., "Comparison of Analysis with Test for Static Loading of Two Hypersonic Inflatable Aerodynamic Decelerator Concepts", NASA/TM-2015-218778, Jul. 01, 2015.
[30] Samareh, J., A., "Estimating Mass of Inflatable Aerodynamic Decelerators Using Dimensionless Parameters." 8th International Planetary Probe Workshop (IPPW-8). Portsmouth, VA. 6-10 June, 2011.
[31] Brown, G. J., "Estimating Minimum Inflation Pressure for Inflatable Aerodynamic Decelerators," AIAA-2009-2970 (revised on June 8, 2009).
[32] Vanessa Dorado, Zachary Grunder, Bryce Schaefer, Meagan Sung, Kevin Pedersen, "NASA Marshall Space Flight Center Tri-gas Thruster Performance Characterization"
[33] Olds, A. D., "IRVE-3 Post Flight Test Reconstruction," AIAA Paper 1514242, Mar 25, 2013.
[34] Overview of the 6 Meter HIAD Inflatable Structure and Flexible TPS Static Load Test Series, IPPW
[35] Johansen, C. T., Novak, L., Bathel, B., Ashcraft, S.W., and Danehy, P. M., "Comparison of MSL RCS jet computations with flow visualization and velocimetry," AIAA Paper 2012-0594, Jan. 9th 2012.